MELTING from an ISOTHERMAL VERTICAL WALL.
Synthesis of a numerical comparison exercise

Dominique Gobin, Patrick Le Quéré

HAL Id: hal-01175159

https://hal-centralesupelec.archives-ouvertes.fr/hal-01175159

Submitted on 15 Jul 2015

MELTING from an ISOTHERMAL VERTICAL WALL.
Synthesis of a numerical comparison exercise.

D. GOBIN[1] and P. Le QUÉRÉ[2]

[1] *FAST - UMR CNRS 7608. Université Paris-Sud. Bât. 502. 91405 - Orsay (France)*

[2] *LIMSI - UPR CNRS 3251. Université Paris-Sud. Bât. 508. 91403 - Orsay (France)*

The compilation of the results presented hereafter has been possible thanks to the participation of the following authors, whose contribution is gratefully acknowledged (affiliations are given in Table 2). Due to space limitations, all the methods are not described in the paper. The interested reader should directly contact the contributors.

B. BASU, R. PARDESHI and A.K. SINGH (`bbasu@pune.tcs.co.in`)

O. BERTRAND and E. ARQUIS (`arquis@lmaster.u-bordeaux.fr`)

B. BINET (`bruno.binet@shadnet.shad.ca`)

H. COMBEAU (`combeau@mines.u-nancy.fr`)

D. GOBIN and G. VIEIRA (`gobin@fast.u-psud.fr`)

J. GOSCIK (`jogoscik@cksr.ac.bialystok.pl`)

M. LACROIX (`marcel.lacroix@gme.usherb.ca`)

P. LE QUÉRÉ (`plq@limsi.fr`)

M. MÉDALE (`medale@iusti.univ-mrs.fr`)

J. MENCINGER and B. ŠARLER (`bozidar.sarler@fs.uni-lj.si`)

H. SADAT and S. COUTURIER (`sadat@let.ensma.fr`)

I. WINTRUFF (`ingo.wintruff@iatf.fzk.de`)

ABSTRACT

This paper provides an analysis of the results of a comparison exercise on the numerical 2D solution of melting from a vertical wall, dominated by natural convection in the liquid phase. The thirteen contributions to this exercise cover the great variety of mathematical models and numerical procedures most commonly used in this field. The main conclusions presented at the AMIF Workshop (PCC99) held in Warsaw in June 1999 and at the Moving Boundaries Seminar in Ljubljana are summarized in the paper. They emphasize the need for the definition of such reference validation tests.

1. INTRODUCTION

The interest for the numerical simulation of the interaction between phase change and fluid flow is motivated by the wide range of industrial or natural processes where the understanding and modeling of such coupling are of importance. The organization of an international workshop on Phase Change with Convection, more specifically dedicated to modeling and validation, reveals the importance of the many developments in this field, and the need for comparing the numerical procedures and results proposed in the heat transfer and mechanical engineering community. The present paper reports a few conclusions concerning a numerical exercise proposed to compare different physical models and numerical procedures applied to a relatively simple phase change problem, where melting is driven by laminar thermal convection in the melt.

This project takes place after several attempts to compare different numerical procedures [1-2]. Existing experimental results are either too limited in the range of parameters [3] or show significant differences between independent studies [4-5]. As a consequence, a purely numerical comparison exercise is proposed, which is intended to provide a set of results in a common framework in order to analyze in detail the characteristics of the numerical solutions in 2D natural convection dominated melting processes, over a wide range of governing parameters. A compilation of the first results may be found in Bertrand *et al.* [6] and the short synthesis proposed in this paper is the second step of such a comparison exercise, based on a larger number of contributions by research teams from different countries. These discussion has been presented in the frame of the AMIF Workshop "PCC99" held in Warsaw in June 1999 and of the "MB99" conference on Moving Boundary Problems held in Ljubljana in July 1999.

2. DESCRIPTION of the EXERCISE

2.1. Problem definition

The problem under consideration deals with melting of a pure substance controlled by natural convection in the melt. One considers a 2D square cavity (height H = width L) initially filled with a solid material uniformly at the melting temperature ($T_0 = T_F$). At t* = 0, the temperature of one of the vertical walls (the left wall in Figure 1) is raised at a value $T_1 > T_F$, while the other vertical wall is maintained at the initial temperature. The horizontal walls are assumed to be adiabatic and no-slip. The fluid flow is supposed to be in the laminar regime, and the thermophysical properties of the material to be constant.

After a pure conduction stage, thermal convection develops in the liquid phase, causing a non-uniform distribution of the heat flux at the interface and a non-uniform displacement of the melting front.

The problem is characterized by a set of four main dimensionless parameters. The fluid phase is defined by its Prandtl number : $Pr = \nu/\alpha$ and the intensity of natural convection is given by the thermal Rayleigh number : $Ra = g\beta(T_1 - T_F)H^3/(\alpha\nu)$. Given the temperature conditions, the Stefan number defines the relative importance of the latent heat in the overall

energy balance : $Ste = C_{PL}(T_1 - T_F)/L_F$. Finally the global aspect ratio of the enclosure has to be specified : $A = H/L$.

2.2. Previous reference results

The above defined problem has been extensively studied in the last twenty years. The existing literature on melting of pure substances driven by thermal natural convection in the melt may be found in various bibliographical compilations [7-9] (for an updated bibliography on the Stefan problem in the LaTeX format, contact Prof. B. Šarler : bozidar.sarler@fs.uni-lj.si). However relatively few experimental results have been reported in the literature and most of them have been dedicated to the qualitative demonstration of the effects of natural convection on the front shape and velocity, or to assess global heat transfer correlations for different geometrical arrangements [10].

A limited amount of papers have been devoted to the constitution of a set of quantitative results, with a precise definition of the boundary conditions and of the thermophysical properties of the phase change material in both the solid and the liquid phase, in order to provide a basis for a comparison with numerical simulations. Two classes of phase change materials have been mainly investigated, leading to different behaviors, according to the properties of the melt:
1. high Prandtl number liquids ($Pr \sim 10^2$), typically paraffin waxes: octadecane, eicosane [3,11-12],
2. in the low Pr domain (Pr $\sim 10^{-2}$), essentially low melting point metals, such as gallium or tin) [4-5,13].
The experimental data are generally produced to validate the numerical procedures developed by the same authors, but some of them (especially [4]) have been used to test the accuracy of independently developed numerical codes. However, due to the many limitations of these experimental studies, the comparison is mainly qualitative and do not meet the requirements for an accurate validation. The main problem lies in the difficulty to control the experimental operating conditions, especially for melting of metals, where the uniformity and time evolution of the wall temperatures, or the importance of the lateral heat losses are scarcely well documented. Besides, the corresponding dimensionless parameters are not necessarily suited to a comparison (usually rather high Rayleigh numbers are considered). Moreover, even when temperature measurements are performed in the system, the relevant experimental data are often restricted to the display of the front position at different times: this information has been proved to strongly depend on the experimental method (the comparison in [5] provides an interesting discussion on this problem).

As a conclusion, the existing corpus of experimental data is adapted only to a first step of the validation of numerical codes, but cannot provide an accurate data base for a quantitative estimation of the computation performance. This appears clearly in the previous attempts to compare distinct numerical methods for the solution of this problem [1,2], where reference to the experimental results by [4] is essentially qualitative.

2.3. Proposed test cases

The consequence of the analysis presented above is two fold:

1. in the absence of reference experiments, purely numerical comparisons must be performed,
2. two groups of numerical tests have to be proposed, corresponding to the distinct Prandtl number ranges.

The governing parameters have been estimated using approximate values of the thermophysical properties of tin and octadecane: in the low Prandtl number range, the Pr value is taken to be 0.02, and in the high Prandtl number range $Pr = 50$. For a given geometry (A = 1), the values of the Rayleigh and Stefan numbers correspond to a dimensional height of the enclosure H = 0.10 m and a reference temperature difference T_1 - $T_F = 3$ ^oC for tin (Case 2) and 10 ^oC for octadecane (Case 4), leading to the values displayed in Table 1 (for more details, refer to [6]). In each Pr range, a 10 times smaller Rayleigh number (Cases 1 and 3) is also considered.

In order to limit the number of outputs, the following results are requested :
1. the time evolution of the melted volume and of the average Nusselt number at the hot wall,
2. the position of the melting front and the local Nusselt number distribution at four different times (expressed in the dimensionless form $\tau = Fo \times Ste = \alpha t^* \times Ste/H^2$) :

- at Pr = 0.02 : $t_1 = 4 \times 10^{-3}$ $t_2 = 10^{-2}$ $t_3 = 4 \times 10^{-2}$ $t_4 = 10^{-1}$,
- at Pr = 50 : $t_1 = 5 \times 10^{-4}$ $t_2 = 2 \times 10^{-3}$ $t_3 = 6 \times 10^{-3}$ $t_4 = 10^{-2}$.

2.4. Heat transfer correlations

After the first attempts to define the characteristic scales of the problem, performed by Webb & Viskanta [14] and Beckermann & Viskanta [15], a complete description of the problem and an analysis of the relevant parameters and scaling laws may be found in the paper by Jany and Bejan [16]. This study leads to the heat transfer correlations described in this section.

In the first stage of the melting process, pure conduction is the dominating heat transfer mechanism. The interface moves parallel to the hot wall, and the time evolution of the front position is given by the classical solution of the Stefan problem (s(t) = 2 $\lambda\sqrt{t}$). Accordingly the Nusselt number decreases like $1/\sqrt{t}$. Then, as the thickness of the liquid layer grows with time, the influence of convection on heat transfer is felt in the top part of the enclosure and progressively along the whole interface. In this transition regime, the competition between pure conduction and natural convection limits the Nusselt number decrease, which goes through a minimum, and then increases when the heat transfer regime is dominated by convection. Finally the boundary layers in the liquid separate and the average heat transfer reaches a constant value.

This analysis was carried out in the high Pr number range, and Jany & Bejan [16] show that the different time scales and heat transfer rates are readily expressed in terms of power laws of the Rayleigh number. The same approach may be extended to the range of low Pr numbers, where the relevant governing parameter is shown to be the dimensionless group Ra × Pr.

The scaling laws lead to correlations for the evolution of the average Nusselt number as a function of time (τ = Fo Ste), the value of the coefficients are identified from the results of numerical simulations.

1. In the range Pr $\ll$ 1 :

$$Nu(\tau) = Nu_\infty + \frac{1}{\sqrt{2\tau}} \left[1 - \frac{1}{\sqrt{1 + \frac{1}{((Ra.Pr)^{0.36}\tau^{0.75})^2}}} \right] . \tag{1}$$

2. In the range Pr $\geq$ 1 :

$$Nu(\tau) = \frac{1}{\sqrt{2\tau}} + \frac{Nu_\infty - 1/\sqrt{2\tau}}{\sqrt{1 + \frac{1}{(0.0175\, Ra^{3/4}\tau^{3/2})^2}}} . \tag{2}$$

where Nu_∞ is given by the expressions $Nu_\infty = 0.33\, Ra^{0.25}$ in the Pr $\gg$ 1 range according to Bénard *et al.* [3] and $Nu_\infty = 0.29\, Ra^{0.27}\, Pr^{0.18}$ in the Pr $\ll$ 1 range [17], or by the more general correlation proposed by Lim and Bejan [18] for any value of Pr :

$$Nu_\infty = \frac{0.35\, Ra^{1/4}}{\left[1 + (0.143/Pr)^{9/16} \right]^{4/9}} . \tag{3}$$

3. CONTRIBUTIONS

13 contributions to the benchmark have been received from academic or industrial research groups, and the corresponding authors and affiliations are listed in Table 2. Contributions using commercial heat transfer softwares have been requested, and complete sets of results are still expected and will be gratefully acknowledged.

Among the sets of results received, only six contributors have solved the four problems. Concerning the melting of metals, eight contributions have solved Case #1, and 12 authors have presented results for Case #2 (2 of them only up to time t_3). In the high Prandtl number range, 11 solutions have been proposed for Case #3 and eight for Case #4. A complete description of each method is not possible in the frame of the present paper. The interested reader will find a short presentation of most methods in [6] and may directly contact the authors. A rapid classification of the main aspects of the numerical procedures follows, summarized by a few keywords in Table 3. In addition, typical mesh size and time step are listed in Table 4 when available.

It may be outlined that the contributions presented hereafter are providing a selection of the most popular models and a variety of alternative numerical procedures. A majority of contributions have used fixed grid or "enthalpy" or one-domain methods (FG), except three (referred as **7,9,13** in Table 2) which have used a front-tracking or transformed grid or two-domain procedures (FT or TG).

One-domain methods (**1-6,8,10-12**)
The common features of these models are the use of the enthalpy formulation for energy conser-

vation and of the primitive variable Navier-Stokes equation for momentum conservation.
The transition from the solid to liquid phase is treated by a Darcy-like penalization term in
the momentum equation depending on the local solid fraction, in all contributions but one, for
which this is handled by a strong viscosity variation in two-phase volumes. The discretization
technique mainly uses the finite volume approach, except two contributions using a finite ele-
ment technique (**3,11**). Structured fixed grids are used in most cases, with the exception of **10**
which uses a moving structured grid to increase the accuracy in the calculation of the flow field
and **3** and **11** where the grid is fixed but eventually non structured.

<u>Front-tracking methods</u> (**7,9,13**)
The common features of these models are the explicit calculation of the front movement and the
use of some kind of upwinding for discretizing the convective terms. A finite volume procedure
with coordinate transformation is used by (**7,9**), while **13** uses a CVFEM approach with an
adaptive unstructured grid. The streamfunction-vorticity formulation is used by **9**, while both **7**
and **13** solve the flow problem in terms of the U-V-P primitive variables. The last main difference
lies in the use of the quasi-stationarity assumption by **7**, while **9** and **13** solve the full transient
flow problem.

4. PRESENTATION OF THE RESULTS

In the short synthesis presented hereafter, the comparison is made separately for the two
ranges of Pr number, and the results are given in terms of the following outputs:
1. time evolution of the average Nusselt number at the hot wall obtained by the contributors.
This is compared to the Neumann solution and to existing correlations recalled above,
2. position of the melting front at four different times of the process.

4.1. The low Prandtl number range (Cases # 1 and #2)

Case # 1 was carried out by eight participants, and all simulations are in good agreement,
as can be seen on the time evolution of the average Nusselt number depicted in Figure 2. This
is obviously due to the fact that at such a low Ra number, melting is dominated by conduction
heat transfer and the evolution is very close to the Neumann solution at Ra = 0. Although no
contribution has presented this test, a comparison of the melted fraction evolution with the $2\lambda\sqrt{t}$
law predicted by the pure conduction solution would have given a useful quantitative element,
since some simulations present some local differences with the analytical solution.

Case # 2 was solved by almost all participants, at least up to t_3. In this case, the quali-
tative difference in the time behaviour of the average Nusselt number already outlined in [6] is
clearly shown in Figure 3-a. Two different classes of time evolutions are observed. A majority
of simulations (**1,2,4,5,7,9,12**) find a Nusselt number evolution very close to correlation (1)
(remember that this correlation has been obtained using a quasi-stationarity assumption, and
the coefficients have been identified from numerical results). Even an amplified display (Figure
3-b) shows a very good agreement of most simulations in this class.

6

The second kind of behavior (in continuous lines in the figure, to allow for the observation of eventual oscillations) gives a significantly higher value of the Nusselt number in given time ranges and present some kind of rapid transient change in the evolution. As first observed in the finite element calculations by Dantzig [19], and confirmed by a recently published stability study [20], this is related to an instability at the end of the conduction regime. This leads to the formation of a multicellular structure and to the successive merging of the upper cells as the melting front advances. The slight quantitative discrepancies between the four solutions leading to this result (**6,10,11,13**) are probably due to differences in the order of accuracy of the space or time discretization scheme.

This is confirmed by the significant differences on the interface position, especially at time $t_3 = 0.04$, as shown in Figure 4-a. The interface positions predicted by the latter four methods (plus method **3**, which is not in this group, as far as the Nusselt number is concerned) are in fairly good agreement, displaying a shape which indicates the presence of two recirculation rolls. At the level of the rolls, the local heat transfer at the interface, and thus the local front velocity are higher. These findings bring a confirmation of the original numerical results by Dantzig, but it must be noted that this behavior has not still been reported experimentally. It thus might be relevant to reconsider some previously published experimental results (see [13], for instance), where it could be possible to find a confirmation of a two-roll structure on the measured front positions.

It is also interesting to note that among the five (probably) more correct solutions, there is no clear-cut superiority of any model or procedure over the others (Figure 4-b): 4 of them are using the enthalpy model, 3 out of five are based on finite volume approximations and structured or non structured meshes, fixed or moving grids are equally used in these solutions.

The differences between the various solutions are slightly smoothed as time proceeds, since the flow regime is monocellular at time t_4, and the front shapes are qualitatively the same. The solutions allowing the observation of the multicellular regime however lead to a faster displacement in the bottom part of the cavity. This may also be seen on the time evolution of the melted fraction (not shown); the dispersion of the results in terms of the liquid fraction at t_4 is less than $\pm 7\%$.

These results however show that the use of a quasi-steady assumption is not permitted in this case, since the flow structure is in continuous evolution as the interface position moves. Extremely small time step is required to capture the flow pulsations, if one relies on the analysis presented in [20]. It seems also clear from the present results that sufficiently fine grids are required to accurately get the multicellular flow structure. This appears clearly from the (limited) quantitative elements shown in Table 4, where information on the time steps and meshes used in the simulations of Case #2 are displayed when available.

As a conclusion of the analysis presented in this section, it seems that the results concerning the description of the dynamics of convective melting of metals from a vertical wall have to be revisited and a more careful and detailed description of the relevant phenomena has to

7

be proposed to the community and confirmed by careful experimental procedures (suggestions may be found in [5]).

4.2. The high Prandtl number range (Cases # 3 and #4)

In the high Pr number range, the stability analysis already mentioned [20] shows that no instability (multicellular flow or oscillatory regime) is to be expected in the range of Rayleigh numbers considered here, and the assumptions leading to the scaling laws established by Jany and Bejan [16] are valid.

The results at $Ra = 10^7$ (Case #3) are displayed in Figure 5-a in terms of the time evolution of the Nusselt number. Although a number of solutions are in a reasonably good agreement in the average, it is clear that some simulations fail to predict the process, and show unrealistic behaviors. Some of them are much too close to the pure conduction solution, while it is well known that the effect of convection at such a Rayleigh number already dominates. Other ones present strong oscillations in the Nusselt number history, which may be attributed to insufficient space resolution: in this case indeed, the enthalpy formulation often leads to such "staircase" steps in the progression of the melting front.
If we discard the extreme behaviors, the seven remaining results displayed in Figure 5-b are relatively close to each other, but the relative differences are nevertheless significant. In the absence of any reference solution, it is difficult to further quantitatively classify the different solutions.

The interface shapes at time t_4 are displayed in Figure 6-a and, as expected, the discrepancies on the local values of the heat transfer are also visible on the melting front position. Interestingly, all methods agree fairly well on the bottom half of the front, while a rather large dispersion may be noticed at the top of the enclosure ($\pm 21\%$ at z = 1), where convective transport is stronger and a good resolution of the dynamic and thermal boundary layers becomes more crucial. Although the selection is arbitrary, 7 among the 11 contributions are in agreement over 75 % of the height, and the dispersion at z = 1 drops to $\pm 9\%$ (Figure 6-b). These differences in the upper part of the enclosure are responsible for the dispersion on the melted fraction ($\pm 10\%$ at t_4 for all results, and $\pm 5\%$ for the 7 selected contributions, not shown).

Note again that there is no clear segregation between the numerical methods: among the three rightmost front positions, almost superposed in Figure 6-b, we find two front tracking results and one fixed grid method, while one FT and 3 FG methods belong to the cluster on the left. One interesting conclusion of this test is the confirmation that the source of the discrepancies lies clearly more in the space (or time) resolution than in the mathematical description of the problem.

At $Ra = 10^8$, the dispersion on the average Nusselt number (Figure 7-a) is similar to the dispersion observed at 10^7, and four solutions out of the eight contributions do not display the central behavior. If we arbitrarily discard these solutions (Figure 7-b), the good overall agreement on the Nusselt number time evolution between the remaining solutions still results

8

in a $\pm$ 4.5 % dispersion on the melted fraction at time t_4 (instead of almost $\pm$ 20 %).

Examination of the melting front position at the largest time ($t_4 = 0.010$) shows a very large variety in the computed shapes of the interface (Figure 8-a). This indicates that, although it corresponds to easily reached experimental conditions, this value of the Rayleigh number is a very demanding numerical test. In this case, the high velocities (strong convective contribution in the transport equations) and the very thin thermal boundary layers (of the order of 10^{-2} in dimensionless terms) may lead to unrealistic results. In this test also, the front position predicted by four simulations out of 8, represented in Figure 8-b, present a very good agreement on the 50 % bottom half of the domain. These correspond to the contributions already selected on the basis of the Nusselt number evolution, giving one more argument for this otherwise arbitrary choice. We must underline that the agreement between these four solutions on the overall shape of the interface is rather qualitative yet, since the dispersion in the front position at the top of the enclosure is still more than $\pm$ 15 % .

Although there is no clear distinction between FT and FG methods in the results of the comparison at high Prandtl and Rayleigh numbers, it must be noted that a similar level of accuracy is obtained with rather lighter grids when FT methods are used. This confirms that the adaptive grids or coordinate transformations allow for an easier description of the thin boundary layers at the interface, where the fixed grid techniques require a much finer space discretization.

5. CONCLUSION

In the absence of any true reference solution to the different cases tested in this exercise, it is difficult to pinpoint in detail the origins of the discrepancies. A few conclusions may be however drawn from the comparison:
1. The simulations at low Pr number tend to confirm the results by Dantzig [19], although, to the authors's knowledge, no evidence of such flow structures and instabilities has been reported in melting experiments so far.
2. The computations at high Prandtl numbers globally indicate the same trends, although they may significantly differ due to grid refinement or to the order of the discretization schemes.
3. In all comparisons, there is no discrimination, as far as the probably most relevant results are concerned, between fixed and transformed grid techniques, nor between classes of discretization methods.
4. In each test, the agreement presented between selected results (Figs. 4-a, 6-a, 8-a) is much better than the comparisons already performed in the past [1-2].
Finally, although many authors have provided information on the CPU time the results have not been presented, due to the extreme diversity of processors used in the computations. A complete evaluation of the codes performance will have to include these data.

As a necessary complementary information to the present corpus of results, and in order to evolve towards the definition of a reference numerical solution to this problem, the participants to the benchmark and future contributors shouild perform a few intermediate tests in the next step of the exercise:

1. check for global energy conservation in the process,
2. verify the accuracy of the solutions in the pure conduction limit. The theoretical values of the λ parameter in the 1D solution ($\lambda_{1(2)} = 0.0705932$ at Ste = 0.01 and $\lambda_{3(4)} = 0.2200163$ at Ste = 0.1) give a basis for a quantitative appreciation of the accuracy in this limit,
3. assess grid and/or timestep convergence of the solutions.
It might eventually be necessary to solve intermediate test problems:
- first, natural convection in an enclosure with a cold vertical wall moving at a prescribed velocity,
- second, phase change problems where a steady-state solution exists. Such a situation is met for instance when the cold wall of the cavity is kept at a lower temperature than the melting point: this case implies the solution of heat conduction in the solid phase and introduces extra parameters, but experimental verification might be easier in the steady state (*e.g.*, see [21]).

Any suggestion or comment will be appreciated.

ACKNOWLEDGEMENTS

REFERENCES

[1] M. Lacroix, V.R. Voller. Finite difference solutions of solidification phase change problems : transformed vs. fixed grids. *Num. Heat Transfer*, B-**17**: 25–41, 1990.

[2] R. Viswanath, Y. Jaluria. A comparison of different solution methodologies for melting and solidification problems in enclosures. *Num. Heat Transfer*, B-**24**: 77–105, 1993.

[3] C. Bénard, D. Gobin, F. Martinez. Melting in rectangular enclosures: experiments and numerical simulations. *J. Heat Transfer*, **107**: 794–803, 1985.

[4] C. Gau, R. Viskanta. Melting and solidification of a pure metal from a vertical wall. *J. Heat Transfer*, **108**: 174–181, 1986.

[5] T.A. Campbell, J.N. Koster. Visualization of solid-liquid interface morphologies in gallium subject to natural convection. *J. Crystal Growth*, **140**: 414–425, 1994.

[6] O. Bertrand, B. Binet, H. Combeau, S. Couturier, Y. Delannoy, D. Gobin, M. Lacroix, P. Le Quéré, M. Médale, J. Mencinger, H. Sadat, G. Vieira. Melting driven by natural convection. A comparison exercise: first results. *Int. Journal of Thermal Sciences*, **38**: 5–26, 1999.

[7] L.S. Yao, J. Prusa. Melting and freezing, *Advances in Heat Transfer* **19**: 1–95, 1989.

[8] R. Viskanta. Heat transfer during melting and solidification of metals. *J. Heat Transfer*, **110**-4B: 1205–1219, 1988.

[9] V.R. Voller. An overview of numerical methods for solving phase-change problems. *Adv. Num. Heat Transfer*, Taylor & Francis, **1**: 341–380, 1997.

[10] M. Bareiss, H. Beer. Experimental investigation of melting heat transfer with regard to different geometric arrangements. *Int. Comm. Heat Mass Transfer*, **11**: 323–333, 1984.

[11] C.J. Ho, R. Viskanta. Heat transfer during melting from an isothermal vertical wall. *J. Heat Transfer*, **106**: 12–19, 1984.

[12] M. Okada. Analysis of heat transfer during melting from a vertical wall. *Int. J. Heat Mass Transfer* **27**: 2057–2066, 1984.

[13] F. Wolff, R. Viskanta. Melting of a pure metal from a vertical wall. *Exp. Heat Transfer*, **1**: 17–30, 1987.

[14] B.W. Webb, R. Viskanta. On the characteristic length scale for correlating melting heat transfer data. *Int. Comm. Heat Mass Transfer*, **12**: 637–646, 1985.

[15] C. Beckermann, R. Viskanta. Effect of solid subcooling on natural convection melting of a pure metal. *J. Heat Transfer*, **111**: 416–424, 1989.

[16] P. Jany, A. Bejan. Scaling theory of melting with natural convection in an enclosure. *Int. J. Heat Mass Transfer*, **31**: 1221–1235, 1988.

[17] D. Gobin, C. Bénard. Melting of metals driven by natural convection in the melt: influence of the Prandtl and Rayleigh numbers. *J. Heat Transfer*, **114**: 521–524, 1992.

[18] J.S. Lim, A. Bejan. The Prandtl number effect on melting dominated by natural convection. *J. Heat Transfer*, **114**: 784–787, 1992.

[19] J.A. Dantzig. Modeling liquid-solid phase changes with melt convection. *Int. J. for Num. Methods Eng.*, **28**: 1769–1785, 1989.

[20] P. Le Quéré, D. Gobin. A note on possible flow instabilities in melting from the side. *Int. Journal of Thermal Sciences*, **38**: 595–600, 1999.

[21] C.J. Kim, M. Kaviany. A numerical method for phase-change problems with convection and diffusion. *Int. J. Heat Mass Transfer*, **35**: 457–467, 1992.

NOMENCLATURE

A	:	aspect ratio of the enclosure, H/L
g	:	acceleration of gravity
Gr	:	Grashof number, $g\,\beta_T\,\Delta T\,H^3/\nu^2$
H	:	height of the enclosure
$\vec{k}$	:	unit vector in the vertical direction
k	:	thermal conductivity of the liquid
L	:	width of the enclosure
Nu	:	average Nusselt number
P	:	dimensionless pressure
Pr	:	Prandtl number, ν/α
Ra	:	Rayleigh number, Pr Gr
Ste	:	Stefan number,
T	:	dimensional temperature
$\vec{V}$	:	dimensionless fluid velocity ($\vec{v}* H/\nu$)
$w\,(u)$	:	vertical (horizontal) component of $\vec{V}$
$x\,(z)$	:	dimensionless coordinates, $x^*/H\ (z^*/H)$

Greek symbols

α	:	thermal diffusivity
β_T	:	coefficient of volumetric thermal expansion
ΔT	:	temperature difference between the heated wall and the interface
λ	:	coefficient of the Neumann solution
ν	:	kinematic viscosity
ρ	:	fluid density
θ	:	dimensionless temperature, $\theta = (T - T_0)/\Delta T$

Pr = 0.02 Ste = 0.01	Case #1 Ra = 2.5 10^4	Case #2 Ra = 2.5 10^5
Pr = 50 Ste = 0.1	Case #3 Ra = 10^7	Case #4 Ra = 10^8

Table 1. Parameters of the test cases.

Author	Laboratory	Test-Cases
1. BASU - SINGH	TRDDC-Pune (India)	1-2-3
2. BERTRAND - ARQUIS	MASTER-Bordeaux (France)	2
3. BINET	IMI-CNRC Boucherville (Québec)	2-3-4
4. BINET - LACROIX	THERMAUS-Sherbrooke (Québec)	2-3-4
5. COMBEAU	LSGMM-Nancy (France)	1-2-3-4
6. COUTURIER - SADAT	LET-Poitiers (France)	1-2-3
7. GOBIN - VIEIRA	FAST-Orsay (France)	2-3-4
8. GOSCIK	Bialystok University (Poland)	3-4
9. LACROIX	THERMAUS-Sherbrooke (Québec)	1-2-3-4
10. Le QUÉRÉ	LIMSI-Orsay (France)	1-2-3-4
11. MÉDALE	IUSTI-Marseille (France)	1-2-3
12. MENCINGER - ŠARLER	LFDT-Ljubljana (Slovenia)	1-2
13. WINTRUFF	IKE-Leopoldshafen (Germany)	1-2-3-4

Table 2. Contributions to the present benchmark.

Contributor	Formulation (1/2 domain)	Method Space scheme	Front description	Misc.
1. BASU-SINGH	U-V-H 1-domain	FVM (UDS) 1st order		Source Term (KC)
2. BERTRAND-ARQUIS	U-V-H 1-domain	FVM (HDS) 1st order		Source Term Penalization
3. BINET	U-V-H 1-domain	FEM (GLS) 1st order	Isotherm 0.015 PCI: 0.015	
4. BINET-LACROIX	U-V-H 1-domain	FVM (HDS) 1st order	$f_S = 0.5$	Source Term (KC)
5. COMBEAU	U-V-H 1-domain	FVM (PLS) 1st order	PCI: 0.1 K $f_L = 0.99$	Source Term (KC)
6. COUTURIER-SADAT	U-V-H 1-domain	Dif. Approx. 1st order		Source Term Penalization
7. GOBIN-VIEIRA	U-V-T 2-domain	FVM (HDS) 1st order	Coordinate Transformation	Quasi-stationarity
8. GOSCIK	U-V-H 1-domain	FVM (PLS) 1st order		Source Term Viscosity variation
9. LACROIX	ψ-ω-T 2-domain	FVM 1st order	Coordinate Transformation	
10. Le QUÉRÉ	U-V-H 1-domain	FVM (CDS) 2nd order	Isotherm 0.001 PCI: 0.001	Multigrid Expanding grid
11. MÉDALE	U-V-H 1-domain	FEM 2nd order	PCI: 0.001	Source Term
12. MENCINGER-ŠARLER	U-V-H 1-domain	FVM (UDS) 1st order	PCI: 0.001 $f_S = 0.5$	Source term Penalization
13. WINTRUFF	U-V-T 2-domain	CVFEM (EDS) 1st order	Explicit	Adaptive grid Triangular

Table 3. Characteristics of the contributions to the benchmark.
Main abbreviations: Upwind (UDS), Power-Law (PLS), Hybrid (HDS) and Exponential (EDS) schemes (see Patankar, 1980); PCI (Phase change interval); KC (Kozeny-Carman model); GLS (Galerkin-Least squares); Finite Element (FEM) or Volume (FVM) Methods.

Contribution	CASE #2		CASE #4	
	δt	Grid NX×NZ	δt	Grid NX×NZ
1.	10^{-4}	60×60 (R)	* 2×10^{-6}	60×60 (R)
2.	10^{-4}	80×80 (R)	—–	—–
3.	2×10^{-4}	41×41	2.5×10^{-6}	41×41
4.	2×10^{-4}	40×40	2.5×10^{-5}	50×181
6.	10^{-5}	202×202	* 2×10^{-6}	122×122
7.	10^{-3}	62×42	10^{-3}	62×42
8.	—–	—–	5×10^{-6}	128×128
9.	2×10^{-4}	21×25	2×10^{-5}	25×35
10.	2×10^{-7}	128×192	10^{-7}	192×192
11.	10^{-4}	100×50 (Q9)	* 10^{-5}	200×100
12.	10^{-6}	100×80 (G)	—–	—–
13.	4×10^{-6}	2000 to 7000	4 to 80×10^{-8}	1100 to 3200

Table 4. Time step and grid size for different contributions and cases #2 and #4.
(*) Only Case #3 has been solved.

FIGURE CAPTIONS

Figure 1. Schematic diagram of the problem.

Figure 2. Case #1 : time evolution of the average Nusselt number at the hot wall.
$(Pr = 0.02 - Ra = 25000 - Ste = 0.01)$

Figure 3. Case #2 : time evolution of the average Nusselt number at the hot wall.
$(Pr = 0.02 - Ra = 250000 - Ste = 0.01)$
a) Full time range
b) Zoom over the t ϵ [0.01-0.03] range

Figure 4. Case #2 : front positions at time $t_3 = 0.040$
a) All simulations
b) Simulations with multicellular flow

Figure 5. Case #3 : time evolution of the average Nusselt number at the hot wall.
$(Pr = 50 - Ra = 10^7 - Ste = 0.1)$
a) All simulations
b) Selection of simulations

Figure 6. Case #3 : front position at time $t_4 = 0.010$
a) All simulations
b) Simulations in agreement over z ϵ [0.-0.75]

Figure 7. Case #4 : time evolution of the average Nusselt number at the hot wall.
$(Pr = 50 - Ra = 10^8 - Ste = 0.1)$
a) All simulations
b) Selection of simulations

Figure 8. Case #4 : front position at time $t_4 = 0.010$
a) All simulations
b) Simulations in agreement over z ϵ [0.-0.5]

Gobin-Le Quéré - Figure 1.

Legend:
◇ Basu - Singh
□ Combeau
⋯⋯ Couturier - Sadat
✕ Lacroix
—— Le Quere
— — Medale
– – – Mencinger - Sarler
-·-· Wintruff
—— Conduction
– – – Correlation
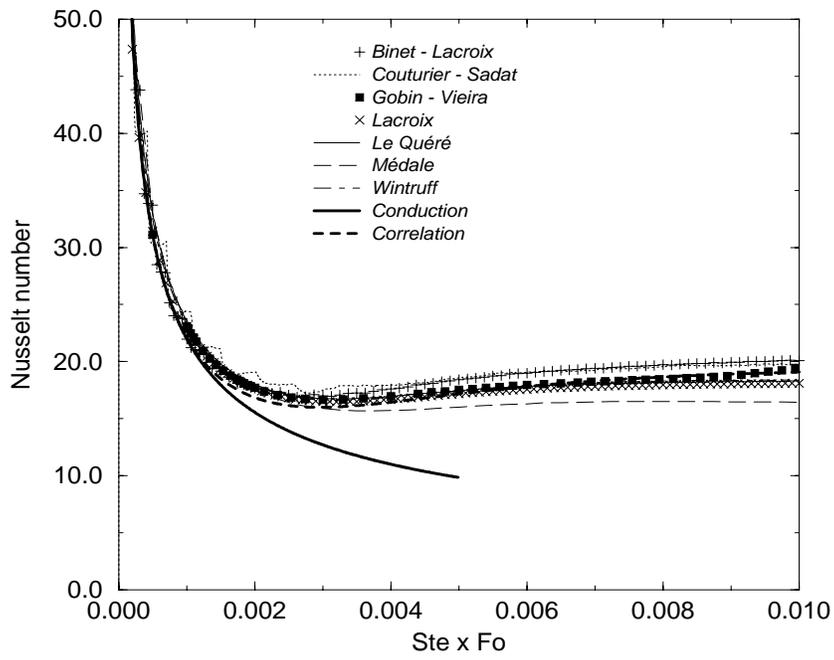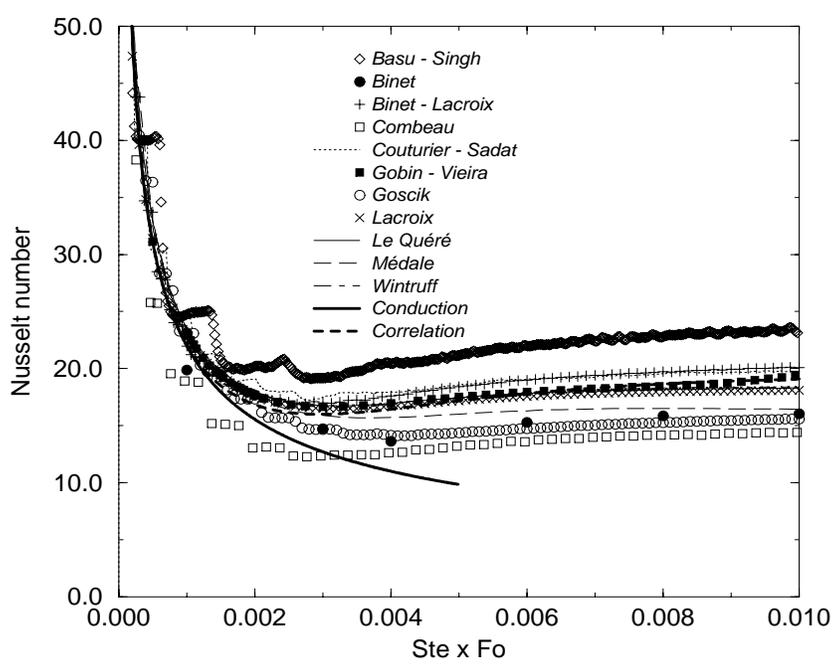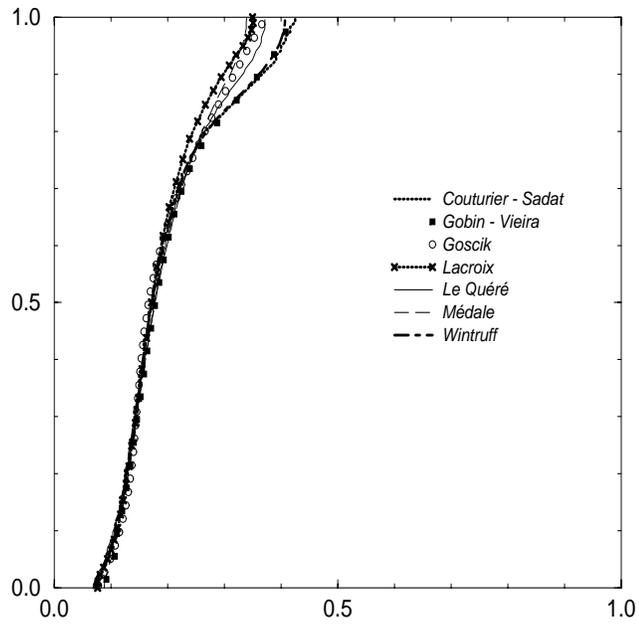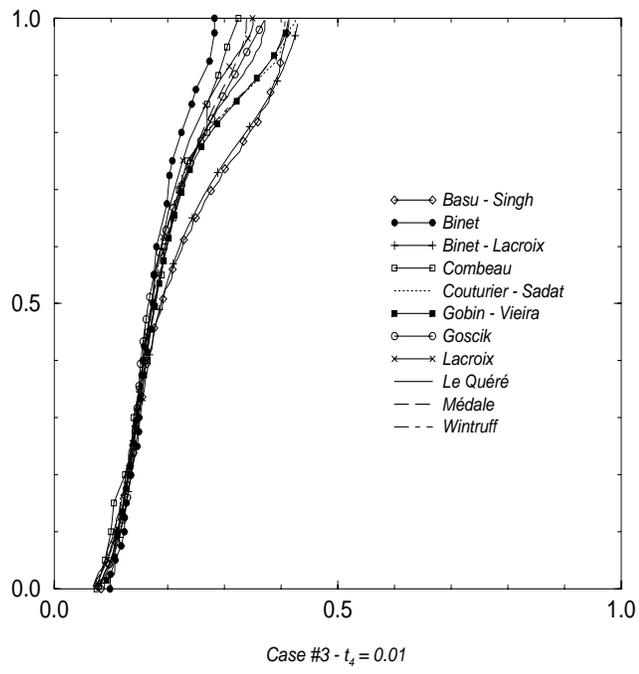
Axes: Nusselt number (y-axis), Ste x Fo (x-axis)
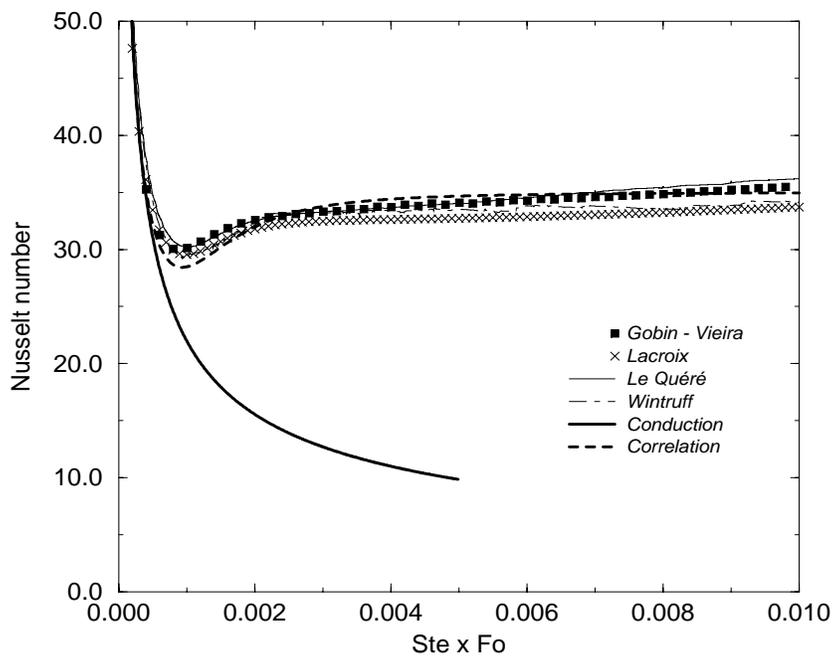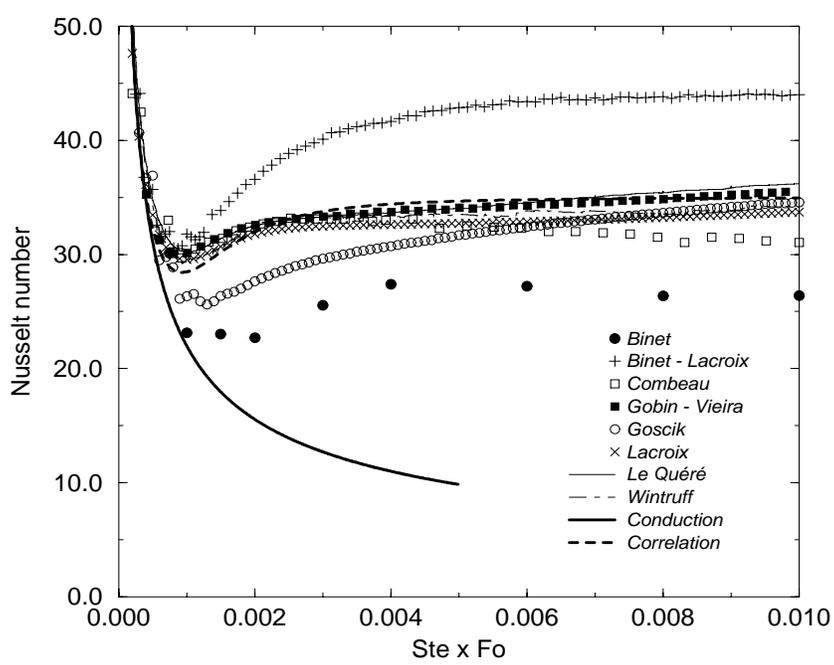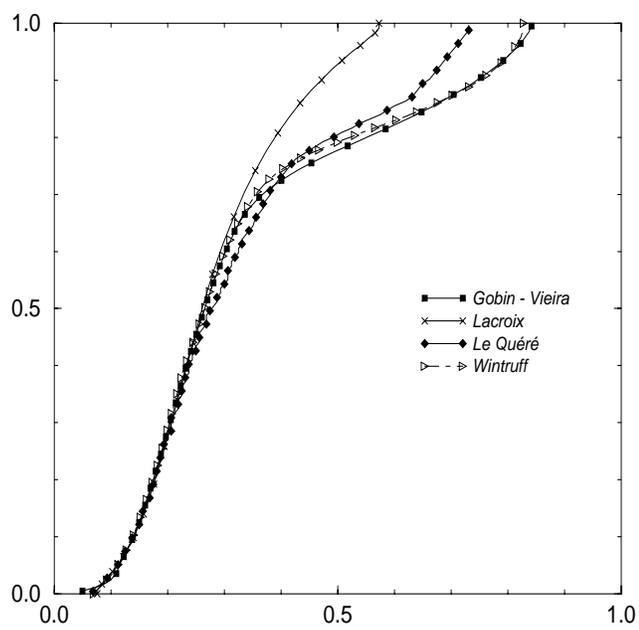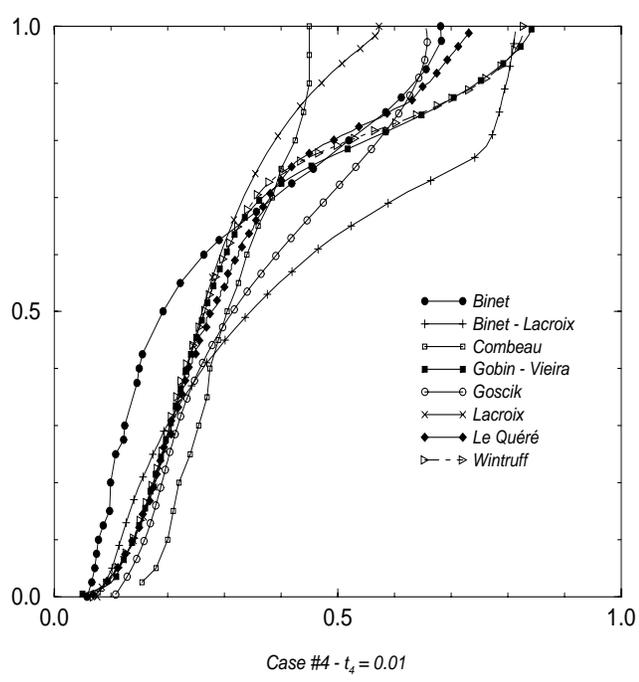
Gobin-Le Quéré - Figure 2.

20
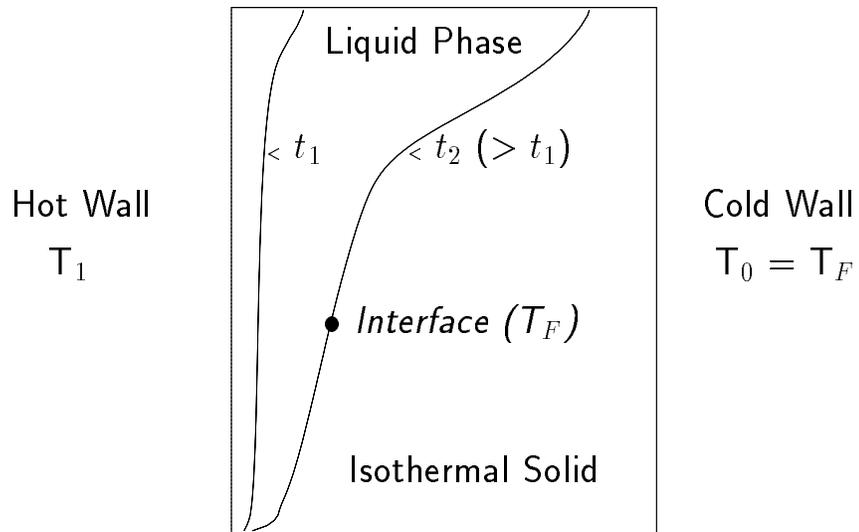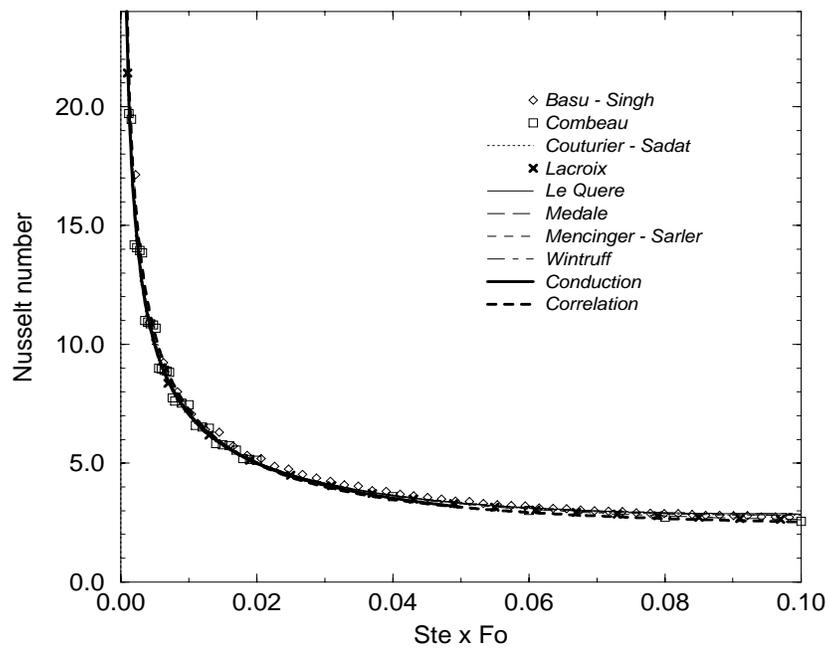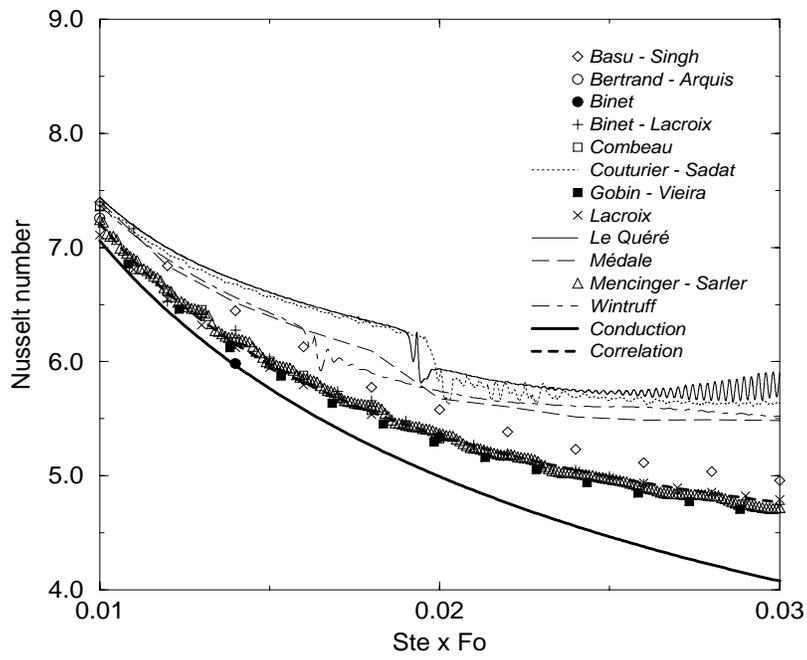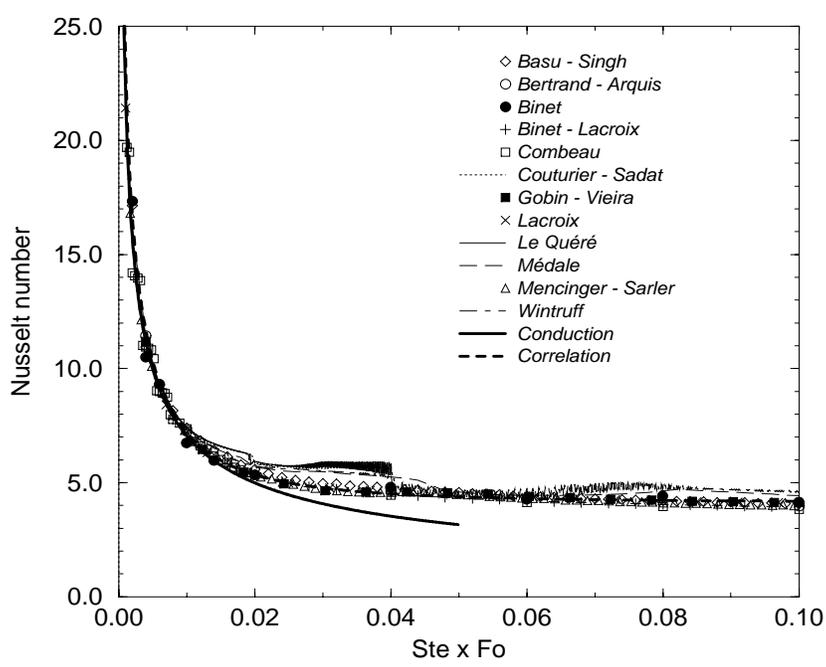
Gobin-Le Quéré - Figure 3.

Case #2 - Time t_3
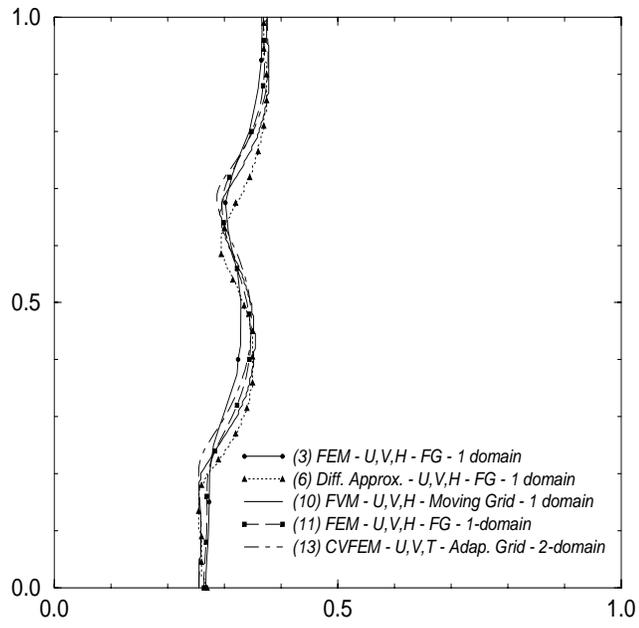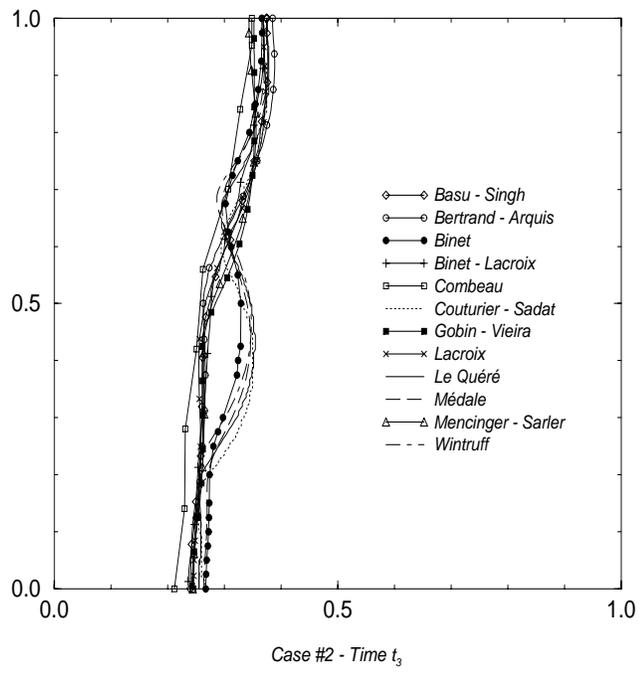
Gobin-Le Quéré - Figure 4.

22

Gobin-Le Quéré - Figure 5.

Case #3 - $t_4 = 0.01$

Gobin-Le Quéré - Figure 6.

Gobin-Le Quéré - Figure 7.

25

Case #4 - $t_4 = 0.01$

Gobin-Le Quéré - Figure 8.